Local temperature measurements in turbulent rotating Rayleigh-Bénard convection

Yuanming Liu and Robert E. Ecke

Phys. Rev. E **84**, 016311 — Published 22 July 2011

DOI: 10.1103/PhysRevE.84.016311

Local temperature measurements in turbulent rotating Rayleigh-Bénard convection

Yuanming Liu[1, 2, *] and Robert E. Ecke[1, 2]

[1] *Center for Nonlinear Studies*
[2] *Condensed Matter and Thermal Physics Group*
Los Alamos National Laboratory, Los Alamos, NM 87545

We present local temperature measurements of turbulent Rayleigh-Bénard convection with rotation about a vertical axis. The fluid, water with Prandtl number about 6, was confined in a cell with a square cross section of 7.3 × 7.3 cm^2 and a height of 9.4 cm. Temperature fluctuations and boundary-layer profiles were measured for Rayleigh numbers $1 \times 10^7 < \mathrm{Ra} < 5 \times 10^8$ and Taylor numbers $0 < \mathrm{Ta} < 5 \times 10^9$. We present statistics of the temperature field measured by a single thermistor located along the vertical centerline of the cell or by an array of thermistors distributed laterally from that centerline. The statistics include the mean temperature, standard deviation, skewness, and the probability distribution functions at various locations in the cell, especially near and inside the thermal boundary layer. The effects of rotation on these quantities are discussed including the presence of a rotation-dependent mean vertical temperature gradient, the negative skewness of temperature fluctuations in the boundary layer, and the horizontal homogenization of temperature.

PACS numbers: 47.27.te, 47.32.Ef, 47.55.P-

I. INTRODUCTION

There is a fascinating interplay between heat transport in rotating convection [1–8] and the vortical nature of structures that arise out of thermal boundary layers at the top and bottom of a Rayleigh-Bénard convection cell [9–12]. Such vortical structures are very familiar in geophysical contexts and have been studied semi-quantitatively in rotating thermal convection experiments with open top surfaces [13]. An important lack in the investigation of rotating turbulent convection is a quantitative understanding of the distribution and spatial organization of the local temperature field although there have been measurements of the vertical temperature gradients in the bulk of the flow [14], *i.e.*, far from solid boundaries. We present local temperature measurements of the thermal boundary layer, the bulk mean temperature gradient, the probability distribution of fluctuations, and the lateral variation of fluctuations and average quantities for rotating and non-rotating convection.

Rayleigh-Bénard convection is characterized by the Rayleigh number Ra which reflects a competition between buoyant forcing and viscous/thermal dissipation and the Prandtl number Pr which determines the dominance of either temperature or velocity in the nonlinearity of convection. Ra is defined in terms of fluid properties as $\mathrm{Ra} = g\alpha d^3 \Delta T/\nu\kappa$ where g is the acceleration of gravity, α is the thermal expansion coefficient, ΔT is the temperature difference across the fluid layer of height d, ν is the kinematic viscosity, and κ is the thermal diffusivity. Similarly, $\mathrm{Pr} = \nu/\kappa$. Properties of turbulent thermal convection are also affected by the geometry of the cell which is characterized by the ratio of a lateral length to a vertical length. For our square geometry, we define the cell aspect ratio as $\Gamma \equiv L/d$ where L is the lateral size of the cell. We report the temperature by subtracting the mean temperature, $T_o = (T_b + T_t)/2$ (where T_b and T_t are the bottom and top temperatures, respectively) and scaling by $\Delta T = T_b - T_t$ to obtain the quantity $\theta = (T - T_o)/\Delta T$. Similarly, the standard deviation σ of the temperature distribution is scaled by ΔT. The vertical distance z measured from the bottom plate is normalized by the cell height to yield z/d. Similarly, the lateral distance x is reported in units of the lateral scale L, *i.e.*, x/L. Using these definitions, θ varies from 0.5 at the bottom boundary to -0.5 at the top boundary with corresponding values of z/d from 0 to 1, and x/L varies from -0.5 to 0.5 (along the diagonal, x/L is between -0.71 and 0.71).

The addition of rotation about a vertical axis introduces a new parameter that measures the effect of the Coriolis force. We use the Taylor number $\mathrm{Ta} = \left(2\Omega d^2/\nu\right)^2$ where Ω is the physical angular rotation rate. For a particular set of the control parameters Ra, Ta, and Pr, the system transports heat through the cell with an efficiency measured by the Nusselt number, the ratio of the effective heat transport from both convective and thermally-conductive processes to the heat transported by thermal conduction alone. The immediate effect of rotation is to suppress the onset of convection because of the Taylor-Proudman condition that suppresses vertical motions in steady, strongly rotating

*Present address: Jet Propulsion Laboratory, California Institute of Technology, 4800 Oak Grove Dr., MS- 79-24, Pasadena, CA

flows [15, 16], leading to the large Ta number result that the critical Rayleigh number varies with Ta as $\mathrm{Ra}_c \sim \mathrm{Ta}^{2/3}$ [17].

For the purposes of understanding the balance of buoyancy and rotation for rotating convection [4, 5], it is useful to introduce the convective Rossby number $\mathrm{Ro} = \sqrt{\mathrm{Ra}/(\mathrm{PrTa})}$ which is a ratio of a rotational time $\sim 1/\Omega$ and a buoyancy time $\sim \sqrt{d/g\alpha\Delta T}$. Rotation dominated flow corresponds to the limit $\mathrm{Ro} << 1$ whereas buoyancy dominated flow typically has $\mathrm{Ro} >> 1$. Because the onset of bulk convection [17] $\mathrm{Ra}_c \sim \mathrm{Ta}^{2/3}$, one cannot obtain a state of rotating convection with arbitrarily small Ro at finite Ta. More precisely, $\mathrm{Ra}_c \approx 7.3\mathrm{Ta}^{2/3}$ so the minimum Ro for a given Ta is $\mathrm{Ro}_m = \sqrt{\mathrm{Ra}_c/(\mathrm{PrTa})} \approx 2.7\mathrm{Pr}^{-1/2}\mathrm{Ta}^{-1/6}$. For $\mathrm{Pr} = 6$ and $\mathrm{Ta} = 10^{10}$, one obtains $\mathrm{Ro}_m \approx 0.03$. If we take a criterion for turbulent convection over the range $10^7 < \mathrm{Ta} < 10^{10}$ as $\mathrm{Ra}_t \approx 2.2\mathrm{Ta}^{0.85}$ [8], one can only achieve a turbulent state of rotating convection for $\mathrm{Ro} \gtrsim 0.1$ for $\mathrm{Ta} \lesssim 10^{10}$.

We previously reported measurements of heat transport of rotating convection in a square convection cell [5, 8] for a fluid with $\mathrm{Pr} \approx 6$. Here we focus on local measurements of the temperature field in the same apparatus. The choice of a square geometry, unusual for studies of rotating convection, was made to better accommodate flow visualization, a feature not used in these experiments. Because container shape can be important in understanding fluctuations for non-rotating convection [18, 19], we note below where geometry may play a role in the interpretation of the results. There have been a number of reports of temperature field measurements in convection without rotation (see, for example, [20–24]), but only a few such experiments [13, 14, 25, 26] and numerical simulations [4, 7, 27, 28] for rotating convection. Without rotation, thermal plumes are generated in thin thermal boundary layers near the top and bottom boundaries where heat enters and exits the convection cell [29, 30]. As rotation forcing increases, as measured by decreasing Ro, the nature of the boundary layer appears to change, leading to modification of the distribution of temperature fluctuations [4, 28] and to enhanced heat transport at moderate Ra and for $\mathrm{Pr} > 2$ [1, 5, 7, 8]. The form of localized disturbances of the boundary layer becomes increasingly vortical for $\mathrm{Ro} < 1$ [3, 4, 11, 25, 31], and the enhancement of heat transport has been attributed to Ekman pumping at the top and bottom boundaries owing to rotation [3, 4, 7, 11, 32]. Note that the absence of Ekman layers in rotating convection for free-slip conditions still leads to a crossover from weak turbulence near onset to stronger rotating turbulence farther from the onset of convection [33]. Another feature of rotating convection at sufficiently high rotation rate is the development of an appreciable mean vertical temperature gradient in the cell interior [4, 7, 14, 28]. In discussing the work presented here, we compare with other experiments and simulations with closed top and bottom boundaries, the preferred geometry for controlled laboratory experiments. We will not consider in any detail work that includes open-top-surface conditions [13, 25, 34, 35], a geometry that is more difficult to measure accurately but which may be more representative of real atmospheric or oceanic flows.

This paper is organized as follows. The experiment is briefly described in Sec. II. The results for temperature fluctuations are presented in Sec. III. Sec. IV provides conclusions and acknowledgements.

II. EXPERIMENTAL PROCEDURE

The experimental apparatus was an improved version of the one used previously in studies of rotating convection [3, 36] and was described in detail elsewhere [8]. Here we concentrate on details of the local probe measurements but review the basic features of the apparatus for convenience. We also review briefly the parameter space of Ra, Ta, and Ro numbers to provide the proper context for subsequent discussions of the results.

A. Rotating convection apparatus and cell

The convection cell was constructed with aluminum top (1.27 cm thick) and bottom (0.64 cm thick) plates and plexiglass sidewalls (0.32 cm thick). The aluminum plates were anodized to prevent corrosion in water. The cell had a height $d = 9.40$ cm and horizontal dimensions $L_x = L_y = 7.30$ cm with an aspect ratio of $\Gamma = L_x/d = 0.78$. Four thermistors were embedded in each plate and gave the average plate temperature. The top-plate temperature and the surrounding cylindrical can that enclosed the cell were temperature regulated with stability and fluctuations of less than 1 mK. A film heater was attached to the bottom plate and provided a constant heat current to the fluid layer. The Rayleigh number was derived from the time-averaged temperature difference between the top and bottom plates with fluid parameters evaluated at the cell mean temperature T_o. The temperature difference corresponding to the highest $\mathrm{Ra} = 4\times10^8$ is about 16 C, the rotation rate Ω corresponding to the highest $\mathrm{Ta} = 5\times10^9$ is 1.57 rad/s, and the Pr number evaluated for $T_o = 21.5$ C is 6.

All electrical wires were fed into the rotating frame through an electrical slip ring and inside a hollow steel shaft which also served as the drive train for rotation. The electrical noise of the slip ring was small enough that there was

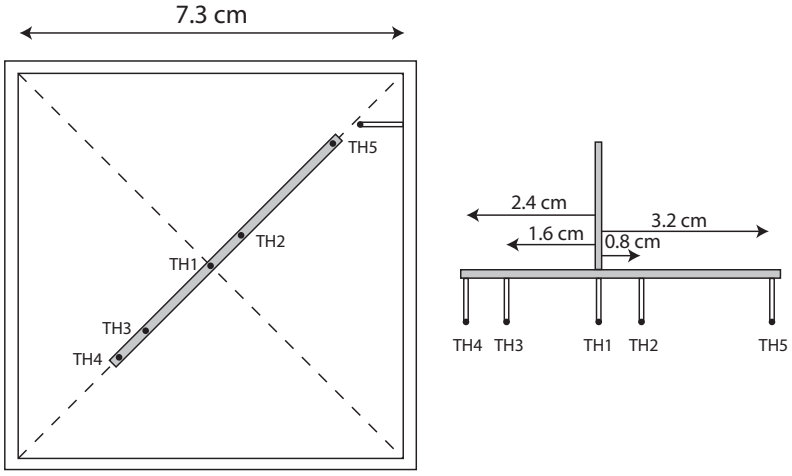

FIG. 1: Schematic top view (left) and side view (right) of the thermistor array. The dimensions, except the sizes of the thermistors, are drawn to scale. The orientation of the thermistor array shown in the left figure is orientation A; orientation B, along the other diagonal, is obtained by rotating the thermistor array clockwise by 90°. The projection of the side thermistor pair in the horizontal plane is also shown in the left figure.

no measurable difference in the signals with or without rotation. Rotation was provided by a micro-stepping motor through a shaft, two gears and a timing belt and was under computer control. The gear ratio set a lower limit for the frequency of about 0.01 Hz. The maximum frequency surveyed was 0.5 Hz.

B. Local temperature measurement

The local temperature of the fluid was measured using a single thermistor or an array of five thermistors. An individual thermistor had a time constant of a fraction of a second, a nominal diameter of 0.035 cm, about 30 k-ohms resistance at room temperature, and a sensitivity of about 1 ohm/mK. The single thermistor or the thermistor array was attached to a 0.15-cm-diameter stainless-steel tube which served as the translation shaft and the electrical feedthrough for the thermistors. The thermistors were moved vertically by a computer-controlled micro-stepping motor with a positional reproducibility of better than 2 μm. Being solid, these temperature probes are not unobtrusive and might affect the flow being measured. Nevertheless, they are similar in construction to other such probes used in thermistor measurements of temperature fields in convection. The position of the probe in the vertical position is measured in units of the cell height, $d = 9.4$ cm, with the bottom plate being at $z/d = 0$ and the top plate at $z/d = 1$.

The thermistor array consisted of five almost identical thermistors and was used to survey the horizontal variation of the temperature field. The thermistors were suspended pointing downwards from a horizontal stainless steel bar with a cross section of 0.25×0.25 cm^2. The tips of the thermistors were about 0.78 cm from the bar. The schematic of the relative positions of the thermistors is shown in Fig. 1 where the five thermistors are labeled for convenience as $TH1$, $TH2$, $TH3$, $TH4$, and $TH5$ with corresponding distances from the center line of 0, 0.8, 1.6, 2.4, and 3.2 cm, respectively. The distance x of the thermistors from the cell centerline is measured in units of the cell lateral side wall, $L = 7.3$ cm, and varies between -0.5 and 0.5 (the positive direction is arbitrarily taken to be in the direction of TH2 and TH5 as in Fig. 1). In these units the positions of the thermistors are $TH1$ ($x/L = 0.0$), $TH2$ ($x/L = 0.11$), $TH3$ ($x/L = -0.22$), $TH4$ ($x/L = -0.33$), and $TH5$ ($x/L = 0.44$). In addition to the movable probe, there was a pair of thermistors located in one corner with distances to the sides of about 0.98 cm and 0.78 cm (shown in Fig. 1). The distance between the lower thermistor and the bottom plate was 3.36 cm (the mid-plane of the cell was at 4.7 cm). The two thermistors were vertically aligned, 0.35 ± 0.01 cm apart. The thermistor array was aligned primarily in two orientations with respect to the side thermistors: orientation A – the thermistor array was aligned along the same diagonal as the side thermistors, and $TH5$ was at the same corner as the side thermistors (shown in Fig. 1); orientation B – the array was rotated clockwise by 90° from orientation A. The side thermistors helped determine the orientation and direction of the mean flow.

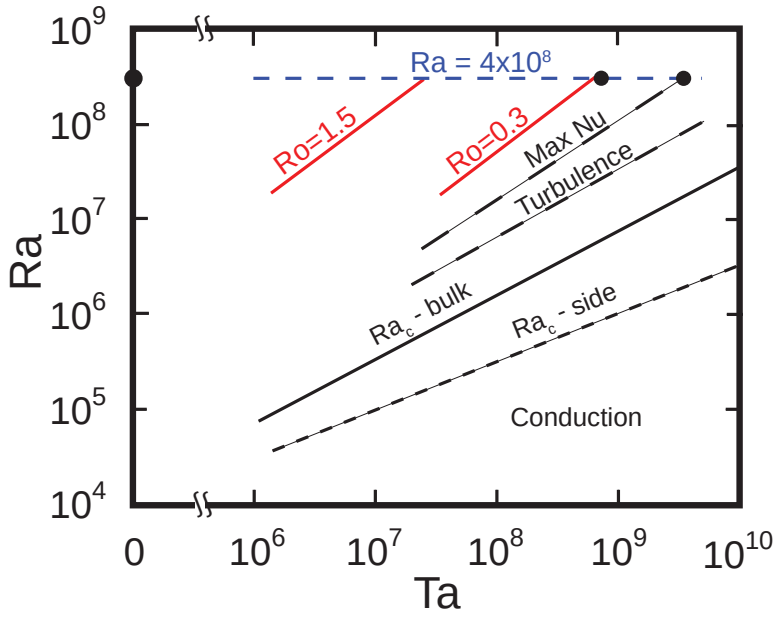

FIG. 2: (color online) Parameter space of Ra vs Ta. Most measurements were conducted along the line Ra = 4×10^8 (dashed line), with special attention (•) given to Ta = 0 (Ro = ∞) and Ta = 5×10^9 (Ro = 0.12). Lines of constant Ro of 1.5 and 0.3 are indicated. Labeled dashed lines indicate approximate loci of maximum Nu at constant Ra, the onset of turbulence, and the Ra_c lines for bulk (solid line) and sidewall convection.

C. Parameter space

The parameter space for rotating convection is defined by Ra and Ta which are proportional to the physical control variables of ΔT and Ω, respectively. In Fig. 2, the parameter space is shown over a range which encompasses our experimental measurements. Measurements of local temperature fluctuations were performed over a small subset of the parameter space covered in the heat transport measurements [8], similar to the path with Ra = 4×10^8 covered in measurements of velocity and vorticity [11].

III. RESULTS

In this section, we present experimental results for local temperature measurements in non-rotating and rotating convection. We first focus on the temperature profile near the cell center, the distribution of temperature fluctuations, and the lateral variation of these quantities. We then focus on the structure of the temperature near the bottom boundary and the relationship between local and global measures of heat transport.

A. Bulk temperature: Fluctuations and mean gradient

Turbulent convection, away from boundary layer regions, produces fluctuating temperature and velocity fields. The statistical properties of the fluctuations are important characteristics of the turbulent motion. One measure of the fluctuations is the probability distribution function (PDF) and its associated moments including the mean, the standard deviation, and the skewness (normalized 3rd moment). Other quantities such as spatial correlations are more difficult to obtain although they are more directly related to turbulence theories. We only consider single-point temperature distributions.

The probability distribution of fluctuations is an interesting probe of turbulence mechanisms in convection with numerous predictions and experimental results for non-rotating convection [20, 37, 38]. In particular, fluctuations in the cell interior reveal details about how thermal disturbances in the boundary layer are advected into the bulk. Although the scaling of such fluctuations with Ra can be affected by the geometry over certain ranges of Ra [18, 19], the form of the distribution of such fluctuations is typically either Gaussian at lower Ra or one with exponential tails

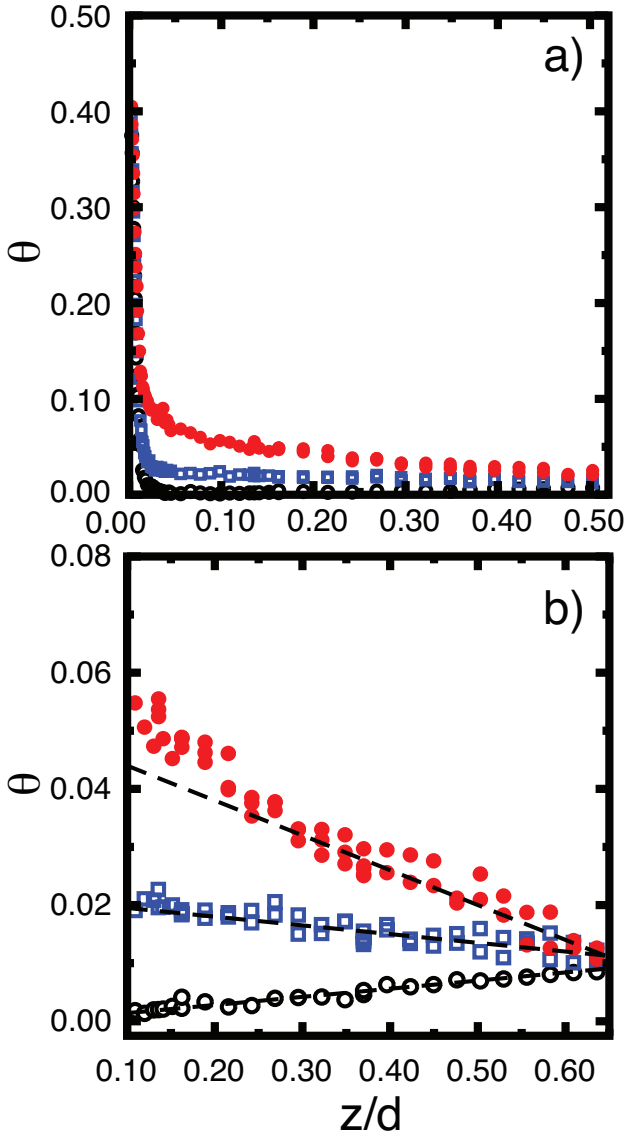

FIG. 3: (color online) a) Full and c)center temperature profile θ vs z/d for Ta = 0 (Ro = ∞, $\circ$), Ta = 3.4×10^7 (Ro = 1.4, $\square$), and Ta = 5.0×10^9 (Ro = 0.12, $\bullet$), respectively. Ra= 4.0×10^8.Dashed lines in b) are fits to the bulk mean gradient $d\theta/dz$.

at higher Ra. We consider, therefore, the evolution of the PDFs in the bulk of the convection cell as a function of rotation rate as measured by Ta or, equivalently, Ro number.

The single thermistor was used to measure the vertical temperature profile from the bottom plate to about 65% of the cell height along the cell centerline as shown in Fig. 3a. The thermistor array was used to study lateral variations of the flow. In either case, the measurement was not non-invasive to the temperature and velocity fields, but the invasiveness is difficult to assess precisely. We discuss below possible issues as they arise.

In the non-rotating turbulent convection observed here, the central region was nearly isothermal and was enclosed by a large scale mean flow. There was a clear transition from Gaussian PDFs at lower Rayleigh numbers, Fig. 4a, to exponential PDFs at higher Rayleigh numbers, Fig. 4b. The transition Rayleigh number for our system was between 2.0×10^7 and 9.2×10^7, consistent with earlier measurements in water [38] and in helium gas [37].

Rotation affects the form and Ra dependence of the temperature PDFs. We obtained PDFs for Ra = 4×10^8 for a set of rotations with Ta listed in Table I. One example is plotted in Fig. 4d for the highest rotation measured (Ta = 5.0×10^9, Ro = 0.12); the other data are very similar in shape. We also made measurements over a range of Rayleigh numbers with constant Ro = 0.30 and 1.2. For both sets of data, no Gaussian-exponential PDF transition was found for Ta = 5×10^9 even when decreasing Ra to as low as 8.7×10^6 (Ro = 0.30) and 1.1×10^7 (Ro = 1.2). Finally, PDFs were measured at Ra $\approx 1 \times 10^7$ for different rotation rates. The PDF at the lowest rotation rate in our experiments

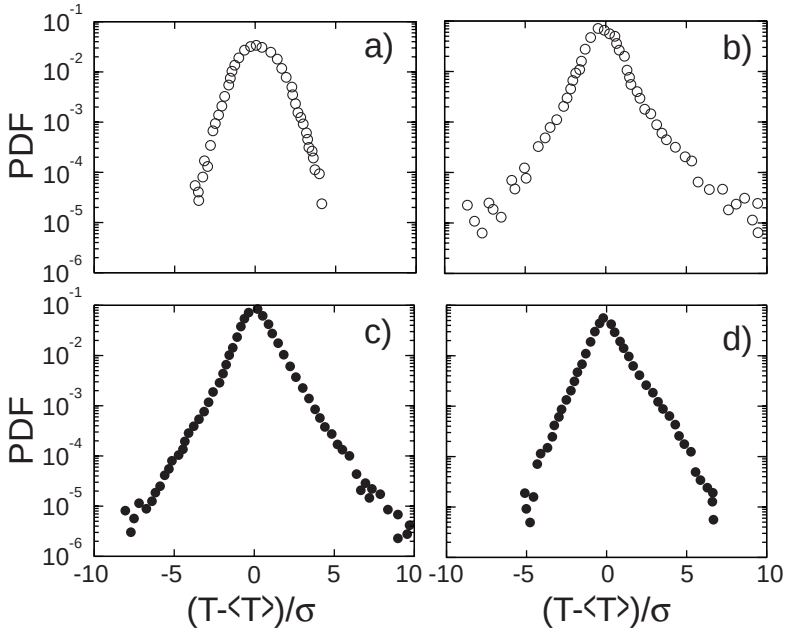

FIG. 4: Temperature PDFs at cell center. Without rotation (Ta = 0, Ro = ∞, ○) for a) Ra = 1.1×10^7 and b) Ra = 4.0×10^8. With rotation (Ro = 0.12, ●) for c) Ra = 1.2×10^7, Ta = 1.4×10^6 and d) Ra = 4.0×10^8, Ta = 5.0×10^9. Notice the transition from Gaussian a) to exponential b) PDFs without rotation. Gaussian PDFs were not observed with rotation (see text).

Ta	Ro	z_0 (cm)	g_0	δ_T/d	z_{max}/d
0.0	∞	0.025	48	0.011	0.009
2.0×10^6	5.8	0.023	45	0.011	0.009
1.3×10^7	2.3	0.023	44	0.012	0.010
3.4×10^7	1.4	0.023	41	0.012	0.010
1.4×10^8	0.69	0.023	39	0.013	0.009
8.1×10^8	0.29	0.025	38	0.013	0.011
2.5×10^9	0.16	0.024	38	0.013	0.011
5.0×10^9	0.12	0.024	34	0.014	0.012

TABLE I: Ta and Ro values for Ra = 4×10^8 where local temperature measurements were performed. Values of z_0 and normalized temperature gradient g_0 are the average values of the fitting parameters over the range $0.0 < z \lesssim 0.05$ cm. The typical error bar for z_0 values is about 0.002 cm. The values of δ_T/d are obtained from the intersection of a straight line fit at small z/d with $\theta = 0$. The values of the peak in the thermal fluctuations z_max/d are also shown for comparison. A different evaluation using the intersection of the small z/d curve with an extrapolation of the mean gradient yields $\delta_T^S/d \approx 0.11$, approximately independent of Ro.

(Ta =1.4×10^6, Ro = 1.2) is plotted in Fig. 4c to compare with the PDF in non-rotating convection at a similar Ra plotted in Fig. 4a; Gaussian PDFs are not observed for rotating convection at these low values of Ra. Temperature fluctuation measurements [26] at higher Ra and Ta than reported here for a fluid with Pr = 8.2 found exponential PDFs for rotating convection at the lower range of Ra but Gaussian PDFs for Ra $\gtrsim 10^{11}$. The evolution of these PDFs with Ra and Ta is complicated (see Fig. 6 in [26]) with PDFs closest to a pure Gaussian form occurring for Ro $\approx$ 2.1 (curiously similar to the transition value of 2.5 from non-rotating heat transport to Ekman enhanced heat transport [7]). For higher Ro, the PDFs are similarly exponential for Ro $\approx$ 10, evolving towards more Gaussian form with only weak Ra dependence. For Ro < 2, there is a return to more exponential PDFs but only slowly with the highest degree of Gaussianity occurring for the large Ra. An extrapolation of this behavior to the lower Ra numbers in this paper is consistent with only observing exponential PDFs.

We also considered the mean and standard deviation of the temperature fluctuation distributions as functions of the vertical and radial coordinates. In Fig. 3a, we show the vertical dependence of the mean temperature $\theta(z/d)$ over the range $0 < z/d < 0.65$ for the Ra = 4.0×10^8 and Ta = 5×10^9 (Ro=0.12). There is a rapid decrease in θ near the boundary and a small variation with increasing z/d. Before considering the boundary layer portion of the

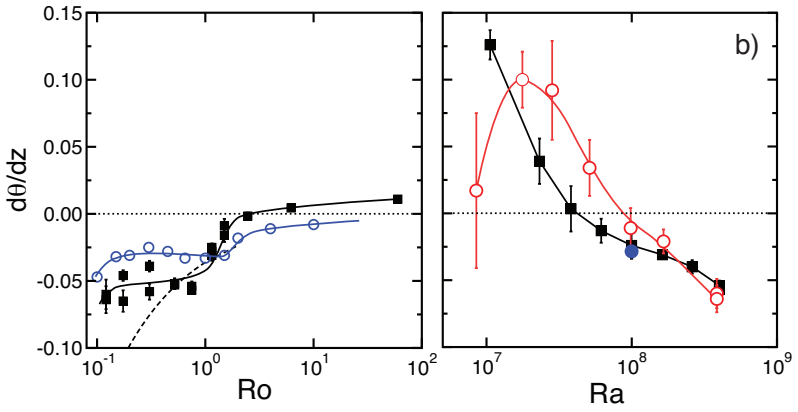

FIG. 5: (color online) $d\theta/dz$ at $z/d = 0.5$ vs a) Ro at constant Ra= 4×10^8 (■) and b) Ra at constant Ro of 0.12 (■) and 0.75 (○). Also included in a) are data from an experiment [14] with Pr = 8.2 and Ra = 1.9×10^{11} (dashed curve) and from a numerical simulations [7] with Pr = 6 and Ra = 1×10^8 (○). The value from this latter curve (about equal values at Ro = 0.12 and 0.75 in a)) is also plotted (●) in b). Solid lines are guides to the eye.

profile, we concentrate on the behavior in the bulk, *i.e.*, near the cell mid-plane. As noted previously [4, 14], the vertical variation of the mean temperature increases with increasing rotation as measured by the vertical temperature gradient $d\theta/dz$ around the cell center. In Fig. 3b, we show the mean temperature profile as a function of z/d over the range $0.1 < z/d < 0.65$ with fits near $z/d = 0.5$ for the mean gradient $d\theta/dz$: The results are plotted in Fig. 5a which shows the dimensionless gradient $d\theta/dz$ as a function of Ro at Ra = 4×10^8. There is a sharp rise when Ro is of order of unity where rotation and buoyancy are comparable in strength. The temperature inversion, *i.e.*, positive gradient, for non-rotating and slowly-rotating turbulence is evident and consistent with experimental measurements that indicate a temperature inversion in square cross section cells but not in cylindrical convection cells [24]. Data from a recent numerical simulation of rotating convection with Pr = 6 and Ra = 1×10^8 [7] are shown for comparison. The trends are quite similar with the magnitude of the negative gradient for the simulations being about half of that for our experiments. The difference can be attributed to the different value of Ra. Fig. 5b shows the gradient as a function of Ra at constant Ro = 0.12 and 0.75. For both values of Ro and at high Ra, the gradient is negative owing to rotation. At moderate Ra, the gradient becomes positive as the result of the temperature inversion. One also sees in Fig. 5b the quite nice correspondence with numerical simulation [7] when the Ra dependence is accounted for. Also in Fig. 5a, we compare with experimental data [14] for rotating convection with Pr = 8.2 and Ra = 1.9×10^{11}. The larger negative gradient at small Ro for these data is consistent with the trend of increasing $d\theta/dz$ with Ra seen in Fig. 5b. For low Ra, near the onset of convection and below our resolution, $d\theta/dz$ should approach -1.

One feature of the center profiles seen in Fig. 3b is that the temperature at the cell center is not the same as T_0, *i.e.*, $\theta(z/d = 1/2) \neq 0$ with larger deviations at higher rotation rates. The asymmetry of θ (positive value) at the mid-plane for non-rotating convection likely results from non-Boussinesq effects which may be substantial because $\Delta T \approx 16$ C for Ra = 4×10^8 [39]. The increase in the thermal offset with rotation, however, may arise from a weak large-scale circulation driven by centrifugal buoyancy [14] in which hotter (cooler) fluid near the bottom (top) of the cell has a net inward (outward) radial velocity that drives an upward flow and thereby advects the warmer bottom fluid in the Ekman layer into the bulk, generating the mean thermal offset. The magnitude of the velocities calculated in this model are small (for Ta = 4×10^9 and Ra = 4×10^8, one has azimuthal velocity $v_\phi < 2 \times 10^{-7}$ cm/s, radial velocity $u_{rad} < 0.01$ cm/s, vertical velocity $w < 1 \times 10^{-4}$ cm/s, see Fig. 4 of [14]), below the resolution of velocity measurements in rotating convection [11]. Nevertheless, the effect on the temperature profile is about the right order of magnitude for the highest Ta [14]. The model requires downward velocities near the wall (to conserve mass) that are confined to thin Stewardson layers with width of order $Ta^{-1/6}d$ which, even accounting for their smaller areal extent, are still quite small, less than 10^{-3} cm/s. In the square geometry used here this centrifugal circulation will be more complex but, as shown below, its presence does explain other features of the local temperature measurements. Because the thermal offset is the largest measurable consequence of the centrifugal buoyancy circulation, it would be worth exploring this feature in other cells with different geometry and different values of Ra and Ta.

In addition to the mean profile $\theta(z/d)$, we computed the standard deviation σ and skewness s of the temperature distributions with the single thermistor probe as functions of z/d, as shown in Fig. 6 for non-rotating (Ro = ∞) and rotating (Ro = 0.12) conditions. There are several dramatic changes with rotation; here we address those near the cell center. First, the standard deviation σ for Ro = 0.12 is much higher than for the non-rotating conditions, see Fig. 6a, about a factor of 5 times higher temperature fluctuations with rotation. Note that there is no obvious way

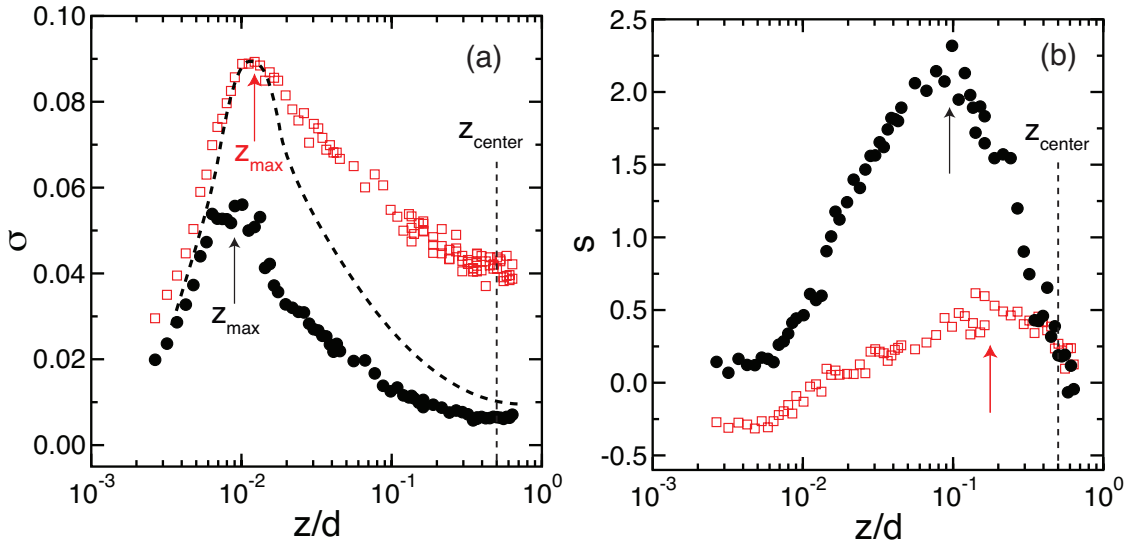

FIG. 6: (color online) a) σ and b) s vs distance from bottom plate z/d for Ra $= 4.0 \times 10^8$ and non-rotating Ta $= 0$ (Ro $= \infty$, •) and rotating Ta $= 5.0 \times 10^9$ (Ro $= 0.12$, □). Vertical arrows in a) and b) indicate vertical positions of the maximum values of σ and s, respectively. Vertical dashed lines indicate vertical cell center position. The dashed curve is the data for Ta=0 scaled to have the same σ_{max} and z_{max}/d as the data for Ro $= 0.12$.

to collapse the data as the rescaled data for the non-rotating case (by the ratio of corresponding values of σ_{max} and z_{max}/d) overlap in the vicinity of the boundary layer but remain very different in the bulk. Second, the skewness s decreases rapidly over the z/d range for both rotating and non-rotating conditions, see Fig. 6b, reaching about the same small magnitude in the range $0.3 < z/d < 0.6$. For smaller z/d, s becomes much larger for non-rotating flows. We discuss the overall evolution of σ and s as functions of z/d below in the context of boundary layer structure.

Temperature fluctuations were measured in the mid-plane with the thermistor array in orientation A (aligned with the mean flow in the non-rotating case) for Ra $= 4 \times 10^8$. Without rotation, the PDF of $TH1$ ($x/L = 0$) was almost symmetric whereas the PDFs of $TH4$ ($x/L = -0.33$) and $TH5$ ($x/L = 0.44$) were skewed towards high and low temperature, respectively. This was presumably caused by the mean flow which was up (hotter) at $TH4$ and down (colder) at $TH5$. Under strong rotation (Ta $= 5.0 \times 10^9$), the asymmetry of the PDFs was much smaller, indicating that the system was homogenized horizontally by rotation. The standard deviation of the fluctuations had a similar trend with lateral distance as seen in Fig. 7 where we plot the ratio $\sigma(x)/\sigma(0)$ as a function of the distance from the centerline. For the non-rotating case, σ/σ_0 increases by over 80% towards the corners where the mean flow is concentrated. The increased σ is likely the result of thermal plumes being swept along the large scale flow leading to a large increase in fluctuations near the wall, see Fig. 7. With rotation, on the other hand, the absence (or weakness) of the large-scale circulation and the vortex form of the thermal structures presumably results in more lateral mixing [4, 11] which would mean larger but more laterally homogeneous fluctuations, as seen in Fig. 7. We revisit the issues of fluctuations and mean gradients after we discuss measurements near the thermal boundary layer. The vertical and horizontal variation of σ are semi-quantitatively consistent with DNS of rotating convection [40].

B. Thermal boundary layer: Thickness, gradient, and fluctuations

In this section, we consider the temperature distributions near the bottom boundary layer, first with the single thermistor to measure the vertical variation of mean and fluctuating quantities and then using the thermistor array to measure the lateral variations of the flow. As measured with the single thermistor, one observes that the structure of the fluctuations near the bottom boundary layer is very different with and without rotation as compared to fluctuations near the cell center. For example, Figs. 4b, d show that at our highest Rayleigh number (Ra $= 4 \times 10^8$) PDFs at the center of the cell do not change much with rotation. PDFs at the same Ra $= 4 \times 10^8$ for values of z/d from within the boundary layer to just outside the boundary layer and for non-rotating and strongly-rotating (Ta $= 5.0 \times 10^9$, Ro $= 0.12$) states are shown in Fig. 8. Inside the boundary layer ($z/d \approx 0.5\delta_T/d$) and without rotation the PDF, Fig. 8a is Gaussian and almost symmetric, or perhaps slightly skewed towards higher temperature, whereas under strong rotation it remains approximately Gaussian, Fig. 8d but skewed towards the low temperature side. This change in

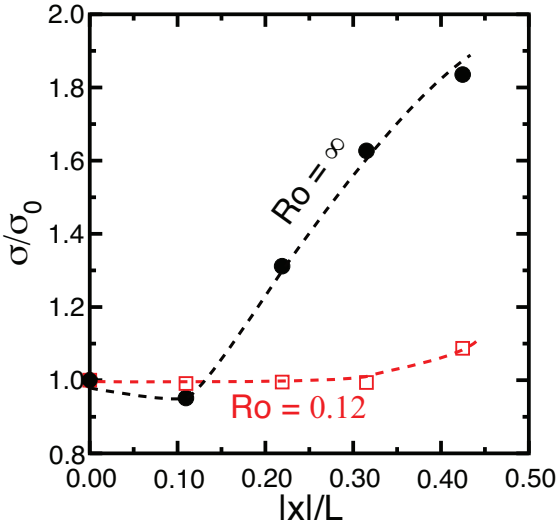

FIG. 7: (color online) Standard deviation σ relative to value at cell center σ_0 vs lateral distance from the centerline ($x/L = 0$) and at mid height ($z/d = 0.5$ for $\mathrm{Ra} = 4.0 \times 10^8$ and $\mathrm{Ta} = 0$ ($\mathrm{Ro} = \infty$, $\sigma_0 = 0.008$, •), $\mathrm{Ta} = 5.0 \times 10^9$ ($\mathrm{Ro} = 0.12$, $\sigma_0 = 0.04$, □). The thermistor array had orientation A. The fluctuation magnitudes are much more laterally homogeneous over the central region with rotation than without.

skewness indicates that under strong rotation colder mixed fluid outside the boundary layer penetrates more deeply into the boundary layer when compared to the non-rotating situation. At $z/d \approx \delta_T/d$ and $2\delta_T/d$, the PDFs without rotation, Figs. 8b,c, have an exponential low-temperature side and are strongly skewed towards higher temperature. With strong rotation, both PDFs, Figs. 8e,f, are Gaussian and almost symmetric. This difference reflects the different nature of thermal plumes and sheets driven across the layer by mean flow without rotation and local vortex motions with rotation. Without rotation, the formation of a thermal plume is rather gradual allowing nearby boundary layer fluid to supply the necessary outgoing mass leading to positive temperature fluctuations whereas negative temperature fluctuations are slightly weaker. The situation is quite different for rotation with Ekman pumping of the boundary layers. One picture, supported by numerical simulation [4] and by lateral velocity experiments [11, 32] in rotating convection, is of an overall vortical motion consisting of lateral flow towards the vortex core but with the possibility of radially outward flow at the vortex core. This circulation pattern would draw bulk fluid into the boundary layer at the core and pump boundary layer fluid into the bulk around some vortex radius. This would help explain the colder fluctuations in the bottom boundary layer. Recently, however, new velocity measurements [41] suggest that the experimental evidence for core suction is an artifact of low spatial resolution. Whether there is core suction or not, Ekman pumping must be sufficiently robust to thin the boundary layer significantly in the vicinity of the vortex, thereby depleting the boundary layer locally and allowing cooler fluid to vertically penetrate the BL region. Further work elucidating the details of the thermal and kinetic boundary layer structure in rotating convection would be helpful in fully explicating the observed change in temperature PDFs in rotating convection.

We now consider the mean of the temperature distribution and its variation near the bottom boundary. With the single thermistor, we measured the boundary layer profile along the cell center line at $\mathrm{Ra} = 4 \times 10^8$ and for values of Ta (Ro) listed in Table I. The linear region inside the boundary layer was fit using $\theta = 0.5 - g_o(z + z0)/d$ where z_0 models the finite size (radius) of the thermistor, and g_o is the temperature gradient normalized by $\Delta T/d$. For the thermistor array, z_0 also takes into account vertical misalignment of each thermistor. The fitted linear range was typically between 0.0 and 0.06 cm. The results are listed in Table I. For the single thermistor, z_0 is fairly constant for all the measurements with an average value close to the thermistor's nominal radius of 0.018 cm (corresponding to $\delta z/d \approx 0.002$). The results presented in the rest of the paper have been corrected by z_0. Data for the temperature profile θ for $\mathrm{Ta} = 0$ ($\mathrm{Ro} = \infty$), $\mathrm{Ta} = 3.4 \times 10^7$ ($\mathrm{Ro} = 1.4$), and $\mathrm{Ta} = 5.0 \times 10^9$ ($\mathrm{Ro} = 0.12$), are plotted in Fig. 9 over the region from $z/d = 0$ to 0.05, about $5\delta_T/d$.

The boundary layer thickness is defined in Fig. 9 in two ways. In the first, the extrapolation of a linear fit for small z/d data to zero defines the boundary layer thickness δ_T. This definition has the advantage that $d\theta/dz = 1/(2\delta_T)$ and is useful for non-rotating turbulent convection because the temperature is essentially constant as a function of height outside the boundary layer. The second definition defines the thickness δ_T^S as the intersection of two straight lines which linearly approximate the regions immediately inside and outside the intersection. This latter definition more accurately defines the width of the boundary layer and has the useful feature here that δ_T^S is approximately

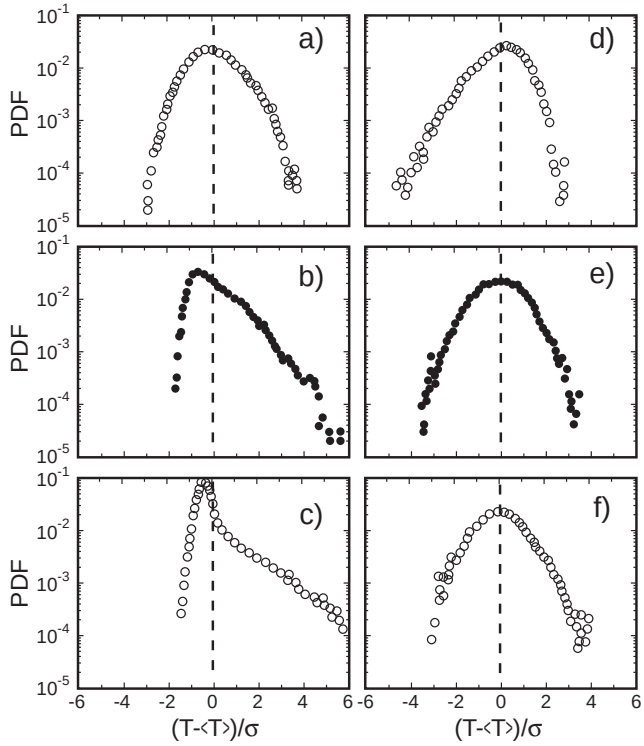

FIG. 8: Temperature PDFs near the bottom boundary layer for Ra $= 4.0 \times 10^8$ and (a-c) Ta $= 0.0$, Ro $= \infty$ (left) and (d-f) Ta$= 5.0 \times 10^9$, Ro $= 0.12$ (right). The distances from the bottom plate z/d are: (a, d) 0.0059 - inside the boundary layer, (b, e) 0.011 - near the boundary layer edge, and (c, f) 0.022 - just outside the boundary layer. Vertical dashed lines accentuate the zero value to emphasize the skewness of the distributions.

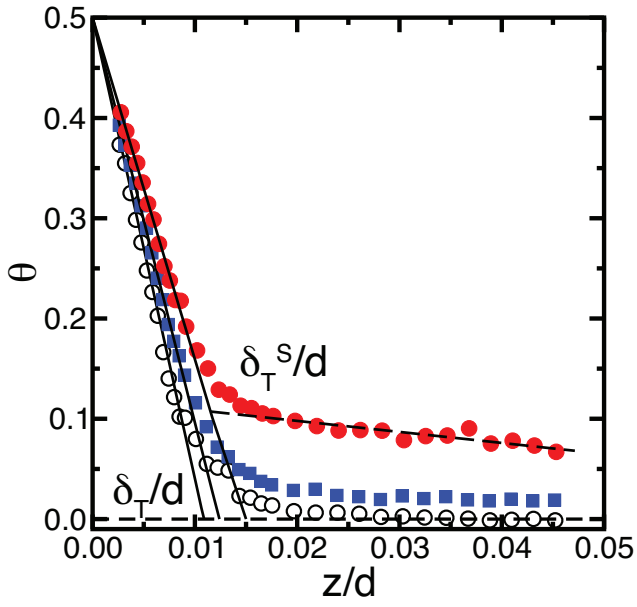

FIG. 9: (color online) Temperature profiles θ vs z/d at Ra$= 4.0 \times 10^8$ and Ta$=0.0$ (Ro $= \infty$, ○), 3.4×10^7 (Ro $= 1.4$, ■), and 5.0×10^9 (Ro $= 0.12$, ●). The lines are guides to the eye.

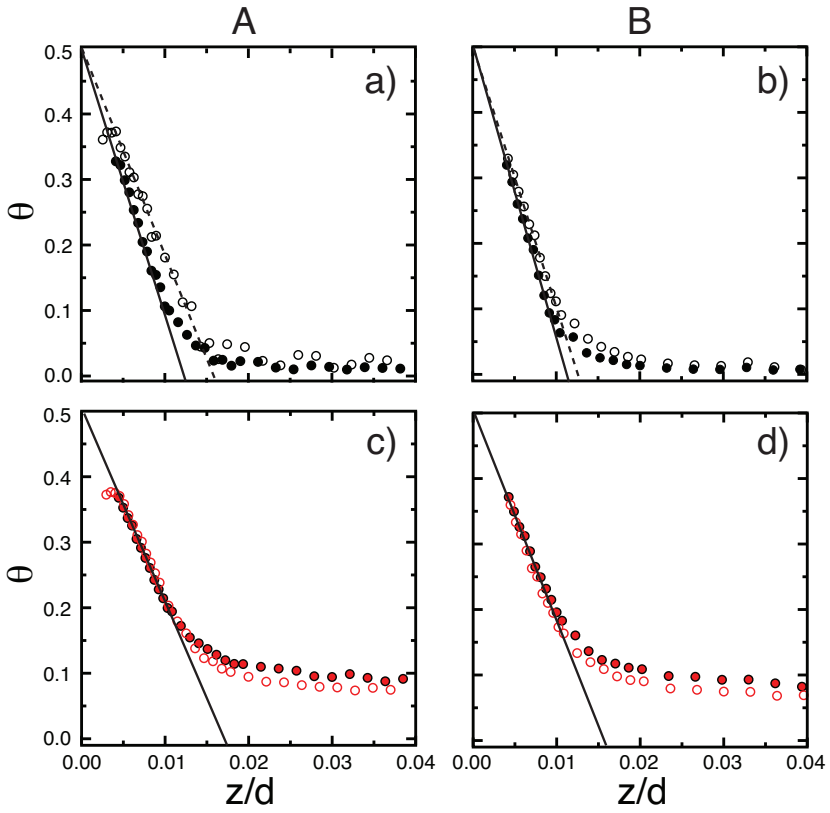

FIG. 10: (color online) Temperature profiles θ vs z/d for Ra $= 4.0 \times 10^8$ for thermistors without rotation (a,b) Ta $= 0$ (Ro $= \infty$) and (c,d) with Ta$= 5.0 \times 10^9$ (Ro $= 0.12$), respectively: $TH1$ ($x/L = 0.0$) (•) and $TH4$ ($x/L = -0.33$) (○). (a,c) Orientation A and (b,d) orientation B. Solid and dashed lines show linear fits to θ for small z/d.

independent of Ro. The boundary layer thickness δ_T is listed in Table I.

We used two orientations of the thermistor array - diagonal orientations A (aligned with the non-rotating mean flow from positive to negative values of x) and B (perpendicular to the non-rotating mean flow direction) - to investigate the lateral variation of the boundary layer. The profile measurements were taken at Ra $= 4 \times 10^8$ and Ta $= 0$ (Ro $= \infty$) and Ta $= 5.0 \times 10^9$ (Ro $= 0.12$). The results can be summarized as showing that without rotation, the mean temperature is more laterally uniform near the cell mid-plane but with larger lateral variation within (or near) the boundary layer. In contrast, the results for rotation indicate a more uniform lateral temperature within the boundary layer with larger variation near the mid-plane.

The temperature profiles obtained from thermistors $TH1$ ($x/L = 0$) and $TH4$ ($x/L = -0.33$) with or without rotation are plotted in Fig. 10 for orientations A (left) and B (right). Without rotation and for both orientations of the array, the values of θ for $TH4$ are higher than for $TH1$ almost everywhere inside and outside the boundary layer, and the slope for $TH4$ is noticeably smaller than for $TH1$ in orientation A, see Fig. 10a. This is consistent with the picture that there is a mean flow in the direction from $TH5$ to $TH4$ for orientation A. The existence of this mean flow was later confirmed by velocity measurements and flow visualization not reported here. Hot thermal plumes are carried along the flow from $TH5$ at one corner to $TH4$ close to the other corner, resulting in higher temperature at $TH4$. Moreover, the smaller slope at $TH4$ indicates that the boundary layer thickens along the mean flow, by about 20-30% from $TH1$ to $TH4$. The large fluctuations in statistical quantities outside the boundary layer without rotation indicate that the flow is irregular as observed in the flow visualization.

Under rotation for both orientations A and B, the temperature profiles in Figs. 10c,d are almost the same inside the boundary layer but the outer thermistors $TH4$ and $TH5$ are colder than the center thermistor outside the boundary layer, *i.e.*, $z/d > 0.02$, contrary to the non-rotating case. Also the data are much smoother outside the boundary layer. This behavior is most likely a result of the weakness or absence of a large-scale mean flow under rotation as indicated in related velocity measurements [11].

In addition to the mean temperature profiles, we extracted other moments of the temperature distributions, namely the standard deviation σ and the skewness s, see Fig. 6. These statistics reflect the state of the turbulent flow. The form

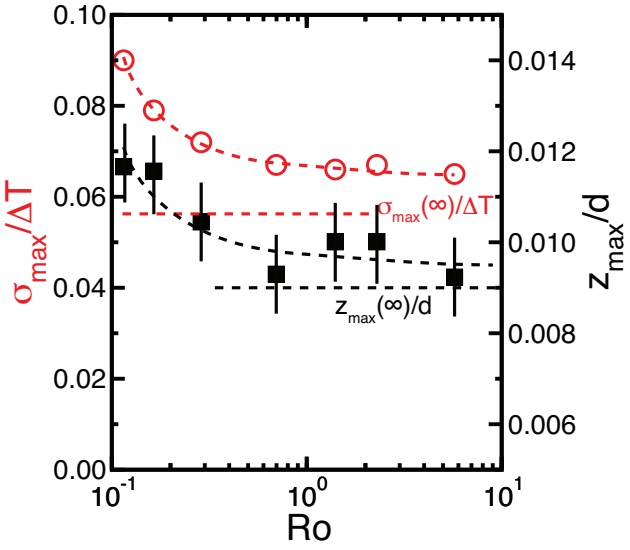

FIG. 11: (color online) σ_{max} (○) and its location z_{max}/d (■) as functions of Ro at Ra $= 4 \times 10^8$. Horizontal dashed lines indicate the asymptotic values for the non-rotating state.

of σ is similar with and without rotation, having similar values within the boundary layer, *i.e.*, $z/d < 0.006 \approx \delta_T/2$, where σ increases rapidly, Fig. 6a. There is a maximum value σ_{max} at $z_{max}/d \approx 0.01 \approx \delta_T$ followed by a gradual decrease towards the cell center. The maxima of σ have larger values with rotation than without. The values of σ_{max} and z_{max}/d are plotted in Fig. 11. From Fig. 6a, one sees that σ under rotation decreases from its maximum less rapidly than without rotation, retaining a much larger value in the interior. Second, the skewness s is smaller under rotation, corresponding to the more symmetric PDFs in Fig. 8d-f, and has negative values inside the boundary layer under rotation as opposed to positive values without rotation, as illustrated by the different symmetries of PDFs in Fig. 8a,d. The positive s without rotation is likely caused by upwelling hot thermal plumes, whereas Ekman pumping may cause the negative skewness under rotation. The large hot and cold fluctuations, actively driven by pumping in the vortex, are also consistent with the larger standard deviation under rotation outside the boundary layer region. Finally, the location of z_{max}/d is about equal to δ_T^S, consistent with edge of the boundary layer being the position of maximum temperature fluctuations with rotation and without rotation.

Since there are large differences in vertical profiles and fluctuations with and without rotation, it is useful to consider their lateral variations. For these measurements we use the thermistor array at several vertical locations. The distances used in the figures below are nominal distances from the bottom plate as the slight alignment problem between the thermistor are not very important far from the bottom boundary. Although the probe structure may interfere with the flow somewhat, we believe that the gross features of the flow are well represented by these measurements.

In Figs. 12 and 13, we show, respectively, θ and σ as functions of the distance away from the cell center line for non-rotating and rotating turbulent convection, different thermistor array orientations, and at two vertical heights $z/d = 0.053 \approx 5\delta_T$ and $z/d = 0.5$. Measurements from the single-thermistor array along the centerline ($x = 0$) are included for comparison, showing good qualitative agreement for data without rotation but deviating somewhat near the boundary layer with smaller θ and larger σ for the rotating case. As noted above, the probe measurements are less reliable owing to alignment and possibly more perturbative of the flow. Nevertheless, the semi-quantitative form of the curves is probably not greatly affected. Without rotation at a vertical height $z/d = 0.053$, the horizontal variations of θ and σ are large under orientation A, and consistent with the picture of a large scale flow from positive to negative and with other measurements in a square geometry [24]; in the flow direction both θ, Fig. 12a, and σ, Fig. 13a, are larger and anti-symmetric. Both variations became smaller under orientation B since the array is perpendicular to the dominant mean flow. The influence of the large-scale flow on both θ and σ near the mid-plane is visible but much smaller. With rotation, θ decreased, Fig. 12b, and σ increased, Fig. 13b, in an approximately symmetric fashion with respect to the centerline with little quantitative dependence on orientation. The lateral variation of θ suggests that the bulk mean gradient is smaller moving out towards the wall: about a 30% reduction for $|x|/L \approx 0.4$ compared to the gradient along the centerline. The maximum in θ at the centerline also suggests an upward warmer flow near the center with a relatively cooler down flow near the walls. The competition of upward flow in the middle and downward flow near the boundary might also account for the increased fluctuations near the lateral boundary for small z/d, see Fig. 13b.

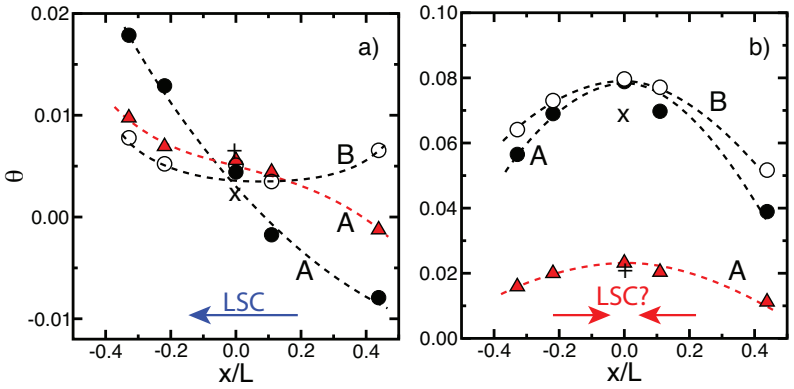

FIG. 12: (color online) θ versus distance from the cell center line for Ra$= 4.0 \times 10^8$ but different rotation rates: a) Ta $= 0$ (Ro $= \infty$) and b) Ta $= 5.0 \times 10^9$ (Ro $= 0.12$). The thermistor array orientation and the distance from the bottom plate are A and $z/d = 0.053$ (•), B and $z/d = 0.053$ (○), A and $z/d = 0.5$ (▲), respectively. Corresponding values from the single thermistor measurements are shown for comparison: $z/d = 0.053$ (×) and $z/d = 0.5$ (+). The lines are guides to the eye. Arrows at the bottom indicate possible large-scale flow circulation consistent with the measurements.

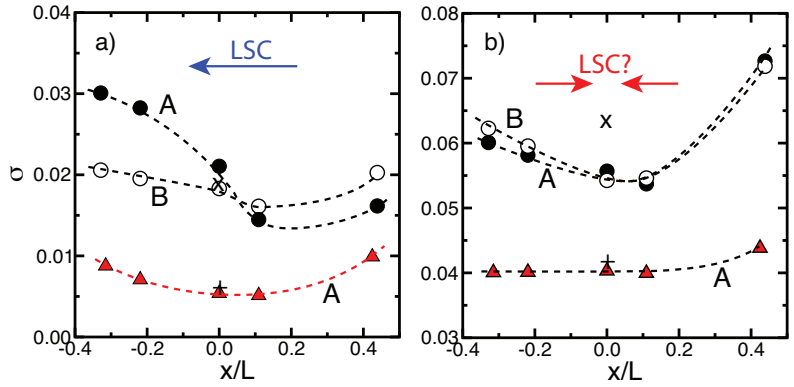

FIG. 13: (color online) σ versus distance from the cell center line for Ra $= 4.0 \times 10^8$ but different rotations: a) Ta $= 0$ (Ro $= \infty$) and b) Ta $= 5.0 \times 10^9$ (Ro $= 0.12$). The thermistor array orientation and the distance from the bottom plate are A and $z/d = 0.053$ (•), B and $z/d = 0.053$ (rotating) and $z/d = 0.041$ (non-rotating) (○), A and $z/d = 0.5$ (▲). Corresponding values from the single thermistor measurements are shown for comparison: $z/d = 0.053$ (×) and $z/d = 0.5$ (+).The lines are guides to the eye. Arrows at the top indicate possible large-scale flow circulation consistent with the measurements.

A local measure of the boundary layer thickness implies a value for the heat transport via the relationship $Nu = d/(2\delta_T)$ (or more precisely via the slope at the bottom (or top) boundary $d\theta/dz$). An analysis of the local temperature measurements gives approximately the right heat transport values but the lateral variation and the lack of measurements in the corners of the square cell make a precise comparison difficult. For example, the area spanned by the lateral probe is only about 50% of the total cross-sectional area of the cell. With these caveats, the local measure of Nu indicates a slightly decreasing heat transport with rotation as opposed to the globally measured small increase in heat transport. Given the measurement uncertainty and the lack of lateral coverage in our probe, a detailed study of this difference is not possible. It would be interesting to measure the boundary layer more systematically in a cylindrical cell where full lateral access to the boundary layer is possible.

IV. CONCLUSIONS

We presented experimental studies of turbulent thermal convection in water confined in a cell with a square cross section with and without rotation. Without rotation, a standard description of turbulent convection applies well. Thermal disturbances in the form of plumes or sheets are generated in thin boundary layers at the cell top and bottom boundaries. These structures produce large fluctuations in the boundary layer with probability distribution functions that are symmetric and Gaussian within the boundary layer, become heavily skewed towards positive fluctuations near

the edge of the boundary layer with an associated maximum in the magnitude of the fluctuations, and become weaker and more symmetric near the cell mid-plane. The skewness of the temperature distribution continues to increase out to about 10 times the boundary layer thickness before becoming symmetric again near the vertical cell center. The turbulence in the bulk leads to very strong vertical homogeneity in the temperature. Finally, the plumes organize themselves into a mean flow that advects fluctuations around the sidewalls, leading to positive and negative skewness of the temperature fluctuations on opposing sides of the cell. The mean flow also affects the boundary layer in the direction of the mean flow by thinning it where fluid of colder or hotter character impacts the oppositely hotter or colder boundary layer and causing thickening as plumes pile up on their journey to the opposite sidewall.

For rotating convection where rotation plays a dominant role, *i.e.*, for convective Rossby numbers less than 1, the temperature fluctuations have a quite different character. Whereas boundary layers persist, their statistical properties vary substantially from the non-rotating case. First, fluctuations are negatively skewed within the boundary layer itself, suggestive of deeper penetration of mean-temperature fluid into the boundary layer via an Ekman pumping mechanism. At the edge of the boundary layer, the PDFs are surprisingly symmetric relative to the very positively skewed non-rotating PDFs at this distance from the bottom boundary. The maximum of σ increases slightly with increased rotation rate, reaching a larger value at its peak - about twice as large for the extremes of non-rotating and strongly rotating turbulent convection. Fluctuations decrease less rapidly towards the cell center for the rotating flow so that the ratio increases from about 2 times to almost 5 times as large for the rotating case. This may result from the absence or different type of mean flow between non-rotating and rotating convection. Whereas the magnitude of fluctuations near the vertical cell center changes by almost a factor of two between the center and the side wall for non-rotating convection, the fluctuations are almost independent of lateral distance. Both the vertical and horizontal dependence of the fluctuations suggests that thermal disturbances advected by the mean flow in the non-rotating flow tend to more concentrated near the boundaries than in the bulk whereas vortical disturbances in the rotating flow ascend vertically and mix laterally leading to larger fluctuations in the bulk with greater lateral homogeneity. A further indication of the tradeoff of vertical and lateral homogeneity in rotating convection is the negative mean gradient that develops for rotating convection as opposed to the slightly positive inversion gradient for the non-rotating flow. Whereas temperature differences θ are qualitatively anti-symmetric with respect to the vertical centerline for non-rotating convection, θ is qualitatively symmetric for rotating convection.

In summary, rotation dramatically changes the nature of turbulent convection in terms of the strong, preferentially cyclonic vortical nature of the plumes formed in the thin top and bottom boundary layers (as opposed to weaker and symmetric vorticity distributions near boundary layers of non-rotating convection [11]). An important topic for future study is the intricate interplay between these vortices and the thermal boundary layer which was raised earlier [4, 11, 12, 32] but remains an open question. Also recent work on the enhancement of heat transport by rotation [7] suggests a diminishing effect at higher Ra, further suggesting that increased Ra would also be of interest in understanding the thermal boundary layer interactions with vortical structures. Rotating convection remains an important and challenging extension to the much studied turbulent Rayleigh-Bénard convection problem and deserves further theoretical, numerical and experimental attention.

Acknowledgments

We would like to thank Joe Werne, Keith Julien, Peter Vorobieff, Phil Marcus, Detlef Lohse, and Richard Stevens for helpful discussions. This work was supported by the U.S. Department of Energy under Contracts W-7405-ENG-36 and DE-AC52-06NA25396. One of us (REE) acknowledges support by the National Science Foundation under Grant No. NSF PHY05-51164 associated with the Kavli Institute for Theoretical Physics Program "Nature of Turbulence."
† Present Address: Low-Temperature Science and Engineering Group, Jet Propulsion Laboratory, 4800 Oak Grove Drive, MS 79-24, Pasadena, CA 91109

[1] H. T. Rossby, J. Fluid Mech. **36**, 309 (1969).
[2] J. M. Pfotenhauer, J. J. Niemela, and R. J. Donnelly, J. Fluid Mech. **175**, 85 (1987).
[3] F. Zhong, R. E. Ecke, and V. Steinberg, J. Fluid Mech. **249**, 135 (1993).
[4] K. Julien, S. Legg, J. McWilliams, and J. Werne, J. Fluid Mech. **322**, 243 (1996).
[5] Y. Liu and R. Ecke, Phys. Rev. Lett. **79**, 2257 (1997).
[6] E. King, S. Stellmach, J. Noir, U. Hansen, and J. Aurnou, Nature **457**, 301 (2009).
[7] J.-Q. Zhong, R. Stevens, H. Clercx, , R. Verzicco, D. Lohse, and G. Ahlers, Phys. Rev. Lett. **102**, 044502 (2009).
[8] Y. Liu and R. Ecke, Phys. Rev. E **80**, 036314 (2009).
[9] G. Veronis, J. Fluid Mech. **5**, 401 (1959).

[10] S. Sakai, J. Fluid Mech. **333**, 85 (1997).
[11] P. Vorobieff and R. E. Ecke, J. Fluid Mech. **458**, 191 (2002).
[12] R. Kunnen, H. Clercx, and B. Geurts, Phys. Rev. E **74**, 056306 (2006).
[13] H. Fernando, R. R. Chen, and D. Boyer, J. Fluid Mech. **228**, 513 (1991).
[14] J. E. Hart and D. R. Ohlsen, Phys. Fluids **11**, 2101 (1999).
[15] J. Proudman, Proc. R. Soc. Lond. A **92**, 408 (1916).
[16] G. Taylor, Proc. R. Soc. Lond. A **93**, 92 (1917).
[17] S. Chandrasekhar, *Hydrodynamic and Hydromagnetic Stability* (Oxford University Press, Oxford, 1961).
[18] Z. Daya and R. Ecke, Phys. Rev. Lett. **87**, 184501 (2001).
[19] H. Song and P. Tong, Europhys. Lett. **90**, 44001 (2010).
[20] X. Z. Wu and A. Libchaber, Phys. Rev. A **45**, 842 (1992).
[21] A. Tilgner, A. Belmonte, and A. Libchaber, Phys. Rev. E **47**, 2253 (1993).
[22] K.-Q. Xia and S.-L. Lui, Phys. Rev. Lett. **79**, 5006 (1997).
[23] Y.-B. Du and P. Tong, Phys. Rev. E **63**, 046303 (2001).
[24] Wang and K.-Q. Xia, Euro. J. Phys. B **32**, 127 (2003).
[25] B. M. Boubnov and G. S. Golitsyn, J. Fluid Mech. **219**, 215 (1990).
[26] J. E. Hart, , S. Kittelman, and D. R. Ohlsen, Phys. Fluids **14**, 955 (2002).
[27] M. Sprague, K. Julien, E. Knobloch, and J. Werne, J. Fluid Mech. **551**, 141 (2006).
[28] R. Kunnen, B. Geurts, and H. Clercx, Euro. J. Mech. B-Fluids **28**, 578 (2009).
[29] E. Siggia, Annu. Rev. Fluid Mech. **26**, 137 (1994).
[30] G. Ahlers, S. Grossman, and D. Lohse, Rev. Mod. Phys. **81**, 503 (2009).
[31] B. M. Boubnov and G. S. Golitsyn, J. Fluid Mech. **167**, 503 (1986).
[32] P. Vorobieff and R. E. Ecke, Physica D **123**, 153 (1998).
[33] S. Schmitz and A. Tilgner, Phys. Rev. E **80**, 015305 (2009).
[34] B. A. Klinger and J. Marshall, Dyn. Atoms. Oceans **21**, 227 (1995).
[35] H. Fernando and D. Smith, Euro. J. Mech.-B/Fluids **20**, 437 (2001).
[36] L. Ning and R. E. Ecke, Phys. Rev. E **47**, 3326 (1993).
[37] F. Heslot, B. Castaing, and A. Libchaber, Phys. Rev. A **36**, 5870 (1987).
[38] T. H. Solomon and J. P. Gollub, Phys. Rev. Lett. **64**, 2382 (1990).
[39] G. Ahlers, E. Brown, , F. A. andD. Funfschilling, S. Grossman, and D. Lohse, J. Fluid Mech. **569**, 409 (2006).
[40] Richard Stevens, Private Communication.
[41] R. Kunnen, H. Clercx, and B. Geurts, Phys. Rev. E **82**, 036306 (2010).